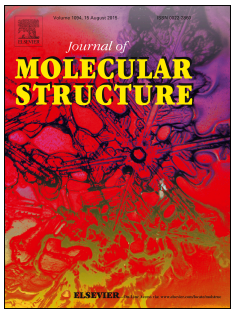

Synthesis, structural peculiarities, theoretical study and biological evaluation of newly designed *O*-Vanillin based azomethines

Muhammad Zubair, Muhammad Sirajuddin, Kaleem Ullah, Ali Haider, Fouzia Perveen, Ishtiaq Hussain, Saqib Ali, Muhammad Nawaz Tahir

PII: S0022-2860(19)31683-7

DOI: https://doi.org/10.1016/j.molstruc.2019.127574

Reference: MOLSTR 127574

To appear in: *Journal of Molecular Structure*

Received Date: 26 October 2019

Revised Date: 29 November 2019

Accepted Date: 11 December 2019

Please cite this article as: M. Zubair, M. Sirajuddin, K. Ullah, A. Haider, F. Perveen, I. Hussain, S. Ali, M.N. Tahir, Synthesis, structural peculiarities, theoretical study and biological evaluation of newly designed *O*-Vanillin based azomethines, *Journal of Molecular Structure* (2020), doi: https://doi.org/10.1016/j.molstruc.2019.127574.

Graphical Abstract: Pictogram

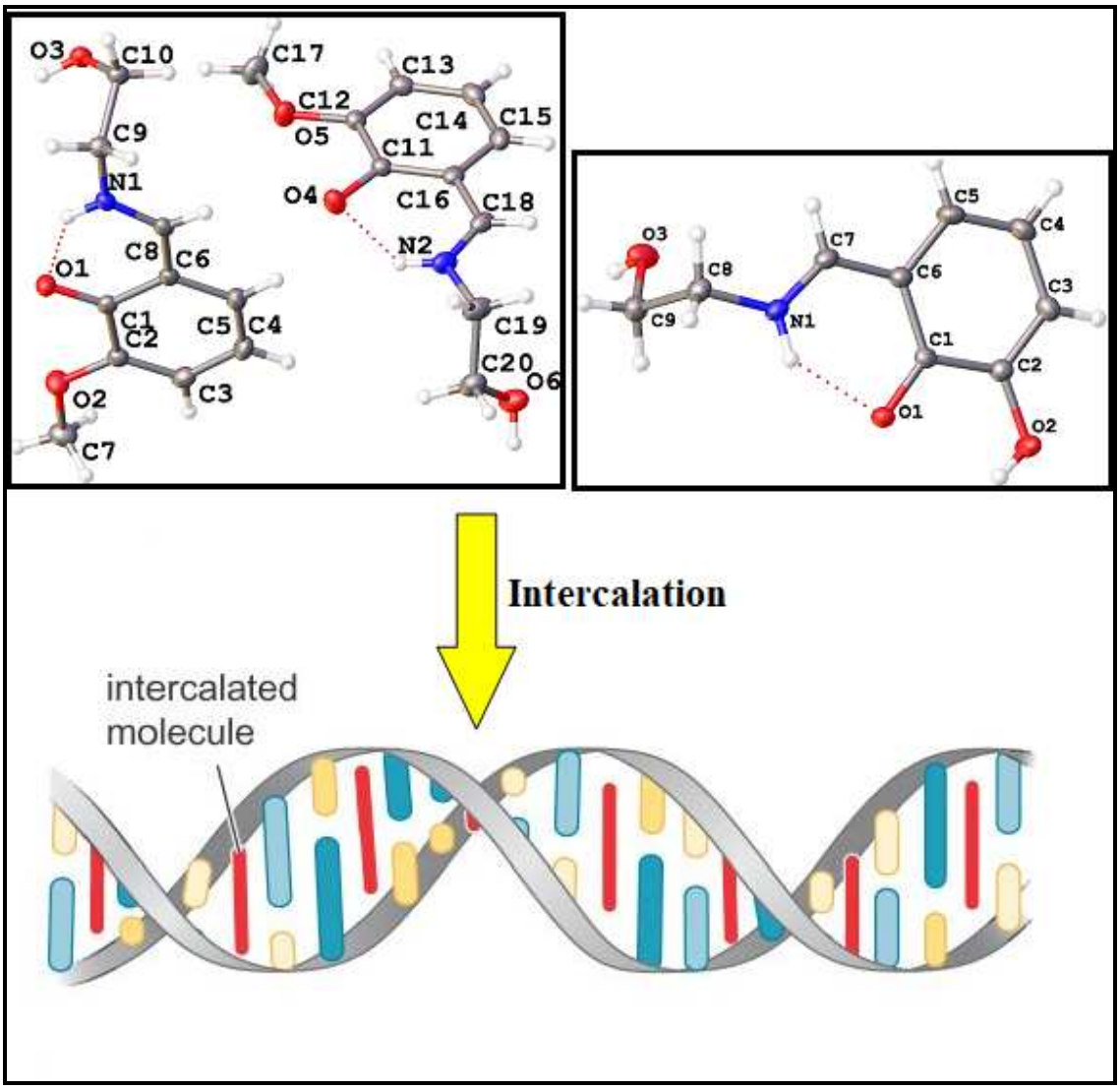

Graphical abstract: Synopsis

The complexes interact with SS-DNA *via* intercalation mode of interaction resulting in hypochromic effect and minor red shift as well as increasing the length of SS-DNA that result in the increase in viscosity of the DNA-compound adduct formed.

Synthesis, Structural Peculiarities, Theoretical Study and Biological Evaluation of Newly Designed *O*-Vanillin Based Azomethines

Muhammad Zubair[a], Muhammad Sirajuddin[b*], Kaleem Ullah[a], Ali Haider[a*], Fouzia Perveen[c], Ishtiaq Hussain[d], Saqib Ali[a*], Muhammad Nawaz Tahir[e],

[a] Department of Chemistry, Quaid-i-Azam University, Islamabad, 45320, Pakistan

[b] Department of Chemistry, University of Science & Technology Bannu, 28100, Pakistan

[c] Research Center for Modeling and Simulations, National University of Science and Technology, Islamabad, Pakistan

[d] Department of Pharmaceutical Science, Abbottabad University of Science and Technology, Havelian Abbottabad, Pakistan

[e] Department of Physics, University of Sargodha, Sargodha, Pakistan

Corresponding Author: A.H.: ahaider@qau.edu.pk, S.A.: drsa54@hotmail.com

Abstract

Two azomethines: (*E*)-2-(((2-hydroxyethyl)imino)methyl)-6-methoxyphenol (**1**) and (*E*)-3-(((2-hydroxyethyl)imino)methyl)benzene-1,2-diol (**2**) were synthesized and characterized in solid state by FT-IR spectroscopy and single crystal X-ray crystallography, whereas in solution state by NMR (^{1}H, ^{13}C) and GC-MS. The titled compounds exist in a zwitter ionic form with a strong intramolecular N–H···O hydrogen bond between the NH^{+} and the phenolate O^{-} as observed both in solution states as well as in solid state. Both the compounds are stabilized in 3D network due to C–H···O, N–H···O and O–H···O types of hydrogen bondings. The optimized molecular geometries were calculated by DFT (density functional theory) with B3LYP functional with 6-31G(d,p) basis set was used using GAUSSIAN 09 program package. The simulated geometries showed excellent correlation with experimentally found structures. The synthesized compounds were investigated for DNA binding interactions using UV-visible spectroscopy and viscometery giving the intercalative mode of interaction with SS-DNA (Salmon sperm DNA). In order to explore the binding modes of compounds with DNA, docking simulations were further performed, that also support the aforementioned results. The compounds were also screened for their *in vitro* antimicrobial activities and the results showed that their antibacterial activity is even higher than that of the standard drug, Cefixime while their antifungal activity is lower than the standard drug, Terbinafine. The interaction of the titled compounds with cetyl trimethy lammonium bromide (CTAB) was investigated by conductometric method to know the critical

micelle concentration (CMC) of CTAB in the absence and presence of compounds. The conductivity measurements revealed higher CMC value in the presence of compounds (For compound **1** CMC = 0.003M while for compound **2** CMC = 0.0031M), proposing a stable compound-CTAB system.

Keywords: Azomethine; Structural elucidation; Molecular docking study; DNA binding study; Antimicrobial evaluation; DPPH activity

1. Introduction

The chemistry of azomethine (Schiff bases) is very generous in providing ligands. The numerous amino and aldo/keto precursors available for condensation reactions leading to azomethine compounds are almost unlimited. The systematic study of the interaction of two starting precursors helps in defining the donor sites, binding mode and number of coordinating ligands [1]. Azomethine based ligands play an important role in the field of inorganic chemistry, as they readily form very stable complexes with many transition as well as main group metal ions in various oxidation states [2-4]. They also have their applications in the field of organic synthesis, dyes and pigments, polymer stabilizers, as catalysts and bio-medicine [5]. Of known aldehydes, *ortho*-vanillin is a naturally occurring and bio-medically active compound that has been widely used as a starting precursor for different azomethines with either mono-donor or multidentate sites. Such ligands are considered as convenient synthetic blocks to coordinate multi-nuclear metals such as trinuclear Gd^{3+}[6] or trinuclear Dy^{3+} [7] with fascinating single molecule magnetic properties [8, 9]. Multidentate Schiff bases are familiar to produce stable complexes, due to coordination through various donor atoms [10]. In coordination chemistry due to their chelating property have been considered as convenient synthetic blocks [11].

The computational chemistry is nowadays a very valuable field in understanding, interpretation and simulation of experimental results like ^{1}H and ^{13}C NMR spectra [12-14] and also very useful for simulation of X-ray geometrical parameters [15, 16]. The binding interactions of the reported compounds are also supported by molecular docking studies. Moreover, quantum chemical calculations are obtained for the synthesized compounds. DFT/B3LYP as function and basis set as 6-31G (d,p) was used in gas phase to optimize the geometry of molecule.

Taking into account the importance of azomethines in different biological fields, herein we have reported the synthesis and spectroscopic investigation of two azomethines derived from 2,3-dihyroxybenzaldehyde (**1**) and *o*-vanillin (**2**). Compound **1** has also been reported by the group

of Tan, where it crystallized in orthorhombic crystal system with space group $Pca2_1$, however, in our case it crystallized in monoclinic crystal system with space group C2/c [17]. Importantly, we investigated the interaction of both compound **1** and **2** with SS-DNA, CTAB as well as their antioxidant and antimicrobial activities has systematically been studied.

2. Materials and Methods

2.1. Synthesis

Ethanolamine, *o*-vanillin and 2,3-dihydroxybezaldehyde were purchased from Aldrich (USA) and were used as received. Sodium salt of SS-DNA were obtained from Arcos and used as such. Solvents used were purchased from Merck (Germany) and dried before use according to the literature procedure [18].

2.2. Physical measurements

Gallenkamp (U.K.) melting point apparatus was used to find the melting point of the synthesized compounds. FT-IR spectrum (4000-400 cm^{-1}) was recorded on a Bruker Tensor II FT-IR Spectrophotometer. ^{1}H and ^{13}C NMR spectra were recorded on a Bruker 300 MHz NMR spectrometer (Switzerland), using DMSO as solvent [δ ^{1}H = 2.5 ppm and ^{13}C = 39.5 ppm]. Single crystal X-ray analysis was performed on a Bruker Kappa APEX-II CCD diffractometer using graphite-monochromated MoKα radiation (λ = 0.71073 nm). The crystal structure was solved by direct methods followed by final refinement on F^2 with full-matrix least-squares using SHELXL-97 [19]. The GC-MS spectra were recorded on a gas chromatograph (GC-6890N) coupled with mass spectrometer having MSD (mass selective detector, model MS-5973). The GC-MS was set to scan in the range of 50-250 *m/z* with electron impact ionization mode. DNA interaction study was performed by using UV-1601 Shimadzu spectrophotometer. Elemental analysis was done using a CE-440 Elemental Analyzer (Exeter Analytical, Inc).

2.3. Synthesis

(*E*)-2-((2-hydroxyethylimino)methyl)-6-methoxyphenol (**1**)

The compound **1** was synthesized by the reaction of equimolar amount of ethanolamine and *o*-vanillin (2-hydroxy-3-methoxybenzaldehyde) in dry methanol using two neck flask equipped with a magnetic stirrer and a condenser (Scheme 1). The reaction mixture was reflux for 2-3 h and was then cooled to room temperature. The reaction mixture volume was concentrated to one third of its original under reduced pressure and kept for crystallization at room temperature. The light yellow crystals suitable for single crystal XRD analysis were obtained after few days.

Yield: 84%; **M.P.** 77-78 °C; **Mol. Wt.**: 195.21 g/mol; **Anal. Calc.** For $C_{10}H_{13}NO_3$ (Found): C, 61.53 (60.92); H, 6.71 (6.74); N, 7.18 (7.10); **FT-IR** (ν, cm^{-1}): 1635 (C=N), 1398 and 1540 (ArC=C), 3398 (free OH), 1217–1346 (Phen. C-O Str. vib.); **^{1}H NMR** (δ ppm): 3.77 (t, H1), 3.49 (t, H2), 4.82 (s, 1H, OH), 8.47 (s, 1H, H3, CH), 13.82 (s, 1H, H5, OH), 3.65 (s, 3H, OCH_3), 6.75 (d, 1H, H7, ^3J [^{1}H, ^{1}H] = 7.8 Hz), 6.77 (t, 1H, H8, ^3J [^{1}H, ^{1}H] = 7.8 Hz), 7.01 (d, 1H, H9, ^3J [^{1}H, ^{1}H] = 7.8 Hz); **^{13}C NMR** (δ ppm): 60.6 (C1), 61.0 (C2), 167.1 (C3), 123.7 (C4), 148.8 (C5), 153.4 (C6), 118.5 (C7), 117.6 (C8), 115.0 (C9), 56.1 (C10). **UV-Vis**: λ_{max}: 409nm.

(*E*)-3-((2-hydroxyethylimino)methyl)benzene-1,2diol (**2**)

Compound **2** was synthesized in similar way as compound **1**, however, reaction was carried out between equimolar concentration of ethanolamine and 2,3-dihydroxybenzaldehyde (Scheme 1).

Yield: 78%; **M.P**. 112-113 °C; **Mol. Wt**.: 181.19 g/mol; **Anal. Calc.**For $C_9H_{11}NO_3$ (Found): C, 59.66 (58.98); H, 6.12 (6.08); N, 7.73 (7.74); **FT-IR** (ν, cm^{-1}): 1647 (C=N), 1354 and 1503 (Ar C=C), 3289 (free OH), 1244–1386 (Phen. C-O Str. vib.); **^{1}H NMR** (δ ppm): 3.65 (t, H1), 3.48 (t, H2), 4.89 (s, 1H, OH), 8.93 (s, 1H, H3, CH), 13.63 (s, 1H, H5, OH), 8.43 (s, 1H, H6, OH), 6.60 (d, 1H, H7 , ^3J [^{1}H, ^{1}H] = 7.5 Hz), 6.79 (t, 1H, H8 , ^3J [^{1}H, ^{1}H] = 7.8 Hz), 6.84 (d, 1H, H9 , ^3J [^{1}H, ^{1}H]= 7.5 Hz); **^{13}C NMR** (δ ppm): 59.4 (C1), 60.9 (C2), 167.1 (C3), 122.3 (C4), 146.9 (C5), 154.5 (C6), 117.3 (C7), 117.7 (C8), 122.3 (C9); **UV-Vis**: λ_{max}: 356nm and 266 nm.

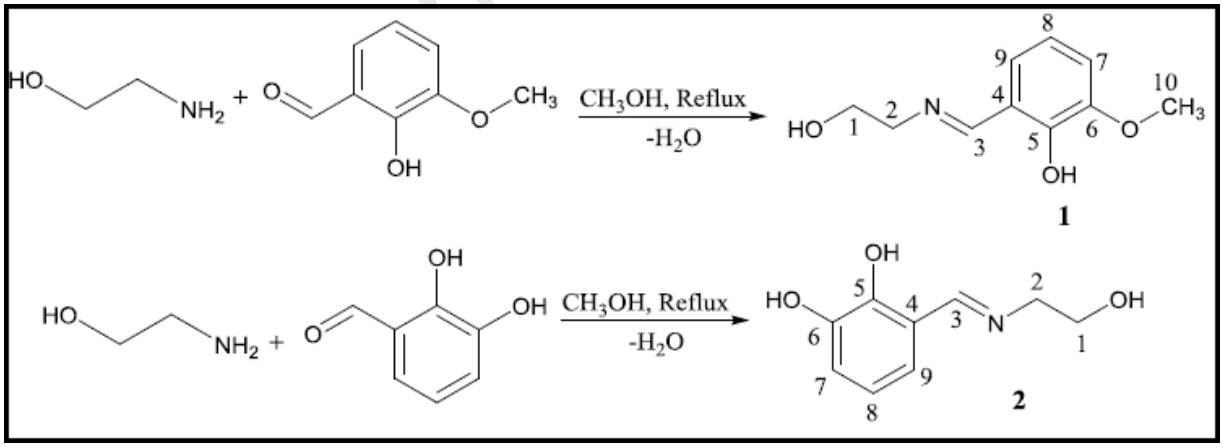

Scheme 1: Synthetic procedure for designing of compound **1** and **2**

2.2.1. DNA interaction studies

DNA solution was prepared by dissolving SS-DNA (20 mg) in deionized water (pH= 7.0) and the solution was stirred for overnight. The prepared solution was stored at 4ºC. The ratio of nucleotide to protein (N/P) of about 1.9 was obtained from the UV-absorbance at 260 and 280 nm (A_{260}/A_{280} = 1.9) which indicates that DNA is free from protein [20]. The concentration of

DNA was calculated to be 1.97×10^{-4} M *via* UV-Vis spectroscopy by applying Beer-Lambert law ($\varepsilon_{SS\text{-}DNA}$= 6600 $M^{-1}cm^{-1}$ at 260 nm) [21] .

The 0.57mM solution of each compound was prepared in 70% ethanol. During the UV visible absorption measurements (1cm path length of cuvettes used), the concentration of SS-DNA was varied while keeping the concentration of the compound fixed. In order to eliminate the absorbance band of DNA, same quantity of DNA was added to both the compound and reference solutions [22]. Prior to each measurement compound-SS-DNA solution was incubated for 25 min at room temperature.

2.2.2. Viscosity measurements

The most reliable and easiest method in defining the compound-DNA binding mode is the viscosity measurement due to its sensitivity towards the change in DNA length as a result of interactions with compound [23]. Herein we performed the viscosity measurements using Ubbelohde viscometer at ambient temperature (25 ± 1 °C). The flow rate was recorded by means of digital stopwatch, where each sample was measured in triplicate. Data of $(\eta/\eta_o)^{1/3}$ was plotted against [Compound]/[DNA] ratio. The η and η_o values represent the DNA viscosity in presence and absence of compound, respectively [24, 25].

2.2.3. Molecular docking

For the purpose of docking simulations molecular structures of compounds **1**and **2** were drawn on MOE-2017 Window employing MOE 2017 tool, entered into MOE database and optimized to minimum energy values employing PM3 semi-emipircal method. 3-D structure of double stranded DNA (PDB. ID: 1D66), was extracted from the RCSB protein Data Bank [26], imported to MOE window, optimized and protonated for further simulation. In order to perform docking analysis, PDB coordinates of 1D66 were optimized to minimum energy employing molecular dynamic AMBER force field and semi-empirical PM3 approaches. These coordinates had minimum energy and stable conformation obtained through MOPAC 7.0. All water molecules were removed from X-Ray crystal structure of DNA. The optimized structures of compounds **1** and **2** were used for methodical conformational search at default limits with RMS gradient of 0.041kJ mol^{-1} *via* Site Finder to find out minimum free energy sites of DNA. Finally the scoring function was used to perform docking studies. To get the best accuracy in the binding docking poses, 30 docking runs were carried out for each compound. The interaction energy of

both compounds **1** and **2** were calculated at every step of the simulation. Where other parameters were set as default [27].

2.2.4. Scavenging effect on 2,2-diphenyl -1-picrylhydrazyl (DPPH)

The antioxidant study is commonly considered as the possible practice used for the treatment of various bio-medical related infections [28]. The antioxidant study of the titled compounds was performed using a 0.089 mM stock solution of DPPH prepared in methanol. Ascorbic acid was used as a standard. To the 2.6 mL solution of DPPH, 0.3 mL of the compounds solutions with concentration ranging from 0.0524 to 1.5 mg/mL were added. After 30 min of incubation, the successive reduction in absorption band of DPPH at 517 nm was examined. Finally, to find the percentage inhibition, the real decrease in absorption was calculated against that of the control, ascorbic acid [29-31]. Each experiment was performed in triplicates to get the precise results.

2.2.5. Computational procedure

The Gaussian 09 program [32] was used to accomplish all the DFT calculations, by applying B3LYP/6-31G level of theory. Moreover, Gauss view 5.0 program package was used to construct the input files (Initial input geometry was constructed from single crystal XRD of compound **1** and **2**) and to plot/ visualize the theoretical results [33, 34]. Additionally, different molecular properties such as highest occupied molecular orbital (HOMO) and lowest unoccupied molecular orbital (LUMO), various thermodynamics properties, chemical reactivity/stability descriptions, electronegativity, dipole moment etc. has also been reported.

2.2.6. Complex–CTAB interaction study by conductometry

The CMC value of CTAB and the effect of compound-CTAB interactions on the CMC value were examined by means of conductometric measurements performed by conductivity meter inolabcond 720 (WTW) calibrated with 3 M KCl solution. The effect on electrical conductivity of compound-CTAB was monitored by keeping the compound concentration constant while changing that of the CTAB.

2.2.7. *In vitro* antibacterial activity

The titled compounds were tested for their antibacterial activity against five different bacterial strains including three Gram-positive: *C. Staphylococci* (*Coagulase-negative staphylococci*), *MRSA* (*Methicillin-resistant Staphylococcus aureus*) and *S. aureus* (*Staphylococcus aureus*) and two Gram-negative: *E. Coli* (*Escherichia coli*) and *K. pneumoniae* (*Klebsiella pneumoniae*) using agar well-diffusion method [35]. DMSO and Cefixime (1 mg/mL) were used as a negative

and positive controls, respectively. Three separate petri plates of every bacterial strain were arranged which were incubated aerobically for 24 h at 37 °C. The average diameter of the zones of inhibition (mm) was calculated as a function of their activity.

2.2.8. *In vitro* antifungal activity

The antifungal activity of synthesized compounds were screened by using agar tube dilution method against various fungal strains including *A. niger, A. fumigatus, A. flavus* and *M. species* [36]. The screw caped test tubes which contain sabouraud dextrose agar (SDA) medium (5 mL) were autoclaved at 120 °C for 20 min. The tubes were allowed to cool slowly at 50 °C and 67 µL of non-solidified SDA was loaded. Then compounds (12 mg/mL in DMSO) from the stock solution were added to make final concentration up to 0.2 mg/mL. The tubes were then allowed to solidify in slanting position (in Laminar flow hood) at room temperature. Each tube was inoculated with 5 mm diameter piece of inoculum from seven days old fungal culture. The media accompanied with DMSO and Turbinafine (200 mg/mL) were used as negative and positive controls, respectively. After 7 days incubation at 27 °C the linear growth was measured (mm).

3. Results and discussion

The desired compounds were obtained in good yields and both were crystallized in methanol. The bulk purity of both compounds was examined by elemental analysis where the results demonstrated good agreement with those of calculated values. The synthesized compounds exhibited sharp melting point showing their purity. The compounds were characterized in solid state by FT-IR spectroscopy and single crystal X-ray diffraction analysis whereas in solution by NMR (^{1}H and ^{13}C) spectroscopy and GC-MS. The structural formula with the tautomeric equilibrium for compounds **1** and **2** are shown in Scheme S1 of the supplementary data. The *Keto-enol* tautomerism can proceed *via enol-imine* as well as *keto-enamine*. In order to verify the proposed tautomers, computational study of both compounds **1** and **2** was performed. In principle, compound **1** can directly undergo *keto-enamine* tautomerization to yield **1** (i), while compound **2** can only undergo *keto-enol* tautomerization to yield 2 (i) as shown in Scheme S1. The binding energies of all the analogues of compounds **1** and **2** were also computed and found that all the analogues are comparatively less stable than the corresponding starting compounds [37].

3.1. Mass spectrometry

The MS spectra of compounds **1** and **2** are shown in Figures S1 and S2 while their mass fragmentation pathways are shown in Schemes S2 and S3 of the supplementary data, respectively. In the mass spectra of both the compounds the parent peaks (molecular ion peak) appeared at m/z = 195 and 181, respectively. The fragments with m/z value 178 and 164 are due to the loss of hydroxyl group from compound **1** and **2**, respectively. Furthermore, the molecular ion peaks go through two other key fragmentation path ways with m/z= 164 and 150 in compound **1** while m/z = 150 and 136 in compound **2**. The fragment of m/z = 164 of compound 1 and m/z = 150 of compound **2** experiences cleavage to give ion peak at m/z = 122 and 109, respectively, by the elimination of C_2H_3N group. This fragment of both the compound yields same fragment m/z = 92 by elimination of methoxy (OCH_3) and (OH) groups from compound **1** and **2**, respectively. This fragment of m/z = 92 of both the compounds undergoes two fragmentation patterns resulting in m/z = 77 and m/z = 65. The former ion peak can be attributed to the phenyl radical ion, while the latter by elimination of CH_2 group via another rout can gives ion peak at m/z = 51.

3.2. Spectroscopic analysis

3.2.1. FT-IR spectroscopy

The detailed FT-IR data for the both the compounds are given in the experimental section. Both the compounds exhibited strong bands in the region of 3500-3200 cm^{-1} attributed to the inter- and intramolecular hydrogen bonded hydroxyl groups which is further supported by the single crystal data. A strong band attributable to azomethine group (C=N) was observed at 1635 cm^{-1} and 1647 cm^{-1}, while the stretching vibration of phenolic C-O band appeared at 1205-1357 and 1244-1386 cm^{-1} in compound **1** and **2**, respectively [38]. Furthermore, for both compounds the stretching vibrations of aliphatic and aromatic C-H group were observed 2914, 3040 cm^{-1} and 2940, 3001 cm^{-1}, respectively.

3.2.2. ^{1}H and ^{13}C NMR spectroscopy

The detailed NMR data for the both the compounds are given in experimental section. The formation of the synthesized compounds **1** and **2** was confirmed by the appearance of a sharp singlet of azomethine proton (N=CH) at 8.47 ppm and 8.93 ppm, respectively. For compound **1**, one of the hydroxyl proton attached to C-1 appeared as a singlet at 4.82 ppm while the other hydroxyl OH attached to the C-5 of the benzene ring appeared at 13.82 ppm. For compound **2**, OH protons attached to C-1 and C-5 appeared around 4.89 and 8.65 ppm, respectively. The

downfield shift of –OH proton attached to aromatic ring (C-5) is due to intramolecular N-H···O hydrogen bonding which is also observed in solid state from single crystal analysis. The formation of the compounds **1** and **2** was further confirmed by ^{13}C NMR giving the peak at 167.1 and 154.5 ppm of the azomethine carbon (C-6). The remaining peaks are found at the positions as calculated by incremental methods as given in the experimental section [39]. The experimental and simulated ^{1}H and ^{13}C NMR chemical shift (DMSO) values of compounds **1** and **2** are reported in Table S1. A good agreement is found in the experimental and simulated chemical shift values.

3.2.3. Single crystal X-ray diffraction study

The crystallographic data and structure refinements parameters are summarized in Table 1 while the various bond lengths and bond angles are given in Tables 2 and 3, respectively. Figures 1 and 2 describe the perspective view of compounds **1** and **2**, respectively. A monoclinic crystal system with space group of C2/c was observed for the both the compounds. Also both the compounds form zwitter ion with the hydrogen of the nearby hydroxyl group and as a result the H of the OH group is transferred from oxygen to nitrogen making a 6-membered stable ring. The stability of the 6-membered ring is due to the strong intramolecular N–H···O hydrogen bond as shown in their structures [17]. The bond lengths and angles are within normal ranges [40] (Allen et al., 1987). The N1=C8 [1.289(2) Å] and N1–C8 [1.457(2)Å] bond distances are comparable to these found in similar Schiff base compounds as reported earlier [17, 41, 42]. In the crystal structures, O3–H3···O1 (Table 4) intermolecular hydrogen bonds formed between the hydroxy and oxygen of phenolate link the molecules into a 3-dimension wave type supramolecular chain structure as shown in Figures S3 and S4 of the supplementary data, respectively. The intra- and inter-molecular H-bondings present in both compounds are shown in Figures S5 and S6 of the supplementary data.

Tables 1-4

Figures 1-2

3.3. Absorption spectral features of DNA-compound binding

UV-Vis absorption spectroscopy is an effective method for studying the DNA-compound interaction and examining the binding mode of compound with DNA. In this method the absorption spectra of free compound and that of compound-DNA are compared to monitor the changes in the absorbance as well as in the peak shifting. In case of intercalation mode of

binding, the compound intercalate into the DNA base pairs where the π orbital of the base pairs of DNA interacts with the π* orbital of the intercalated aromatic chromophore, therefore, reducing the π→π* transition energy and causes bathochromic shift. Additionally hypochromism is observed because of the partially filled electrons in π orbital of intercalated compound that reduces the probabilities of transition and accompanying in the hypochromism. Therefore, hypochromism when coupled with bathochromism the intercalation mode of binding between compound-DNA occurs [43].

The compounds reported in the manuscript are small organic molecules for which DNA is the easy target as mentioned in the literature. Moreover these compounds are structurally analogue to compounds binding to DNA *via* various mode of interaction [44]. Figures 3 and 4 demonstrate the absorption spectra of the investigated compounds in the absence (a) and presence (b-m) of SS-DNA. For free compound **1** there exists one strong peak at about 409 nm while for compound **2**, two peaks were observed at 356 nm and 266 nm. With incremental addition of DNA, the absorption bands exhibit hypochromism and small bathochromism (red shift) of about 4 nm. All these observations give a clue that the synthesized compounds bind with DNA *via* an intercalative binding mode [45]. Furthermore, the extent of compound-DNA interaction was evaluated in term of binding constant (K) that was determine using the intercept-to-slope ratio of $A_o/(A-A_o)$ *vs.*1/[DNA] plots. The observed values of binding constant for the investigated compounds are 1.7×10^4 M^{-1} and 1.36×10^4 M^{-1}, respectively. The spontaneity of the DNA-compound adduct formation process was evaluated from the negative value of Gibbs free energy (ΔG) using the equation [46]:

$\Delta G = - RT\ln K$

Here R = 8.314 $Jmol^{-1}K^{-1}$ and T = 298 K. The values of ΔG calculated for the screened compounds are -24.13 kJ mol^{-1} and -23.58 kJ mol^{-1}.

Figures 3-4

3.4. Viscosity measurements

Viscosity or hydrodynamic measurements response to the change in length of DNA during interactions with compounds, therefore, it is considered as most simplest and more reliable method to describe the interaction mode of DNA-compound [47]. During the intercalative mode of binding, DNA lengthens due to the accumulation of compound between the base pairs resulting in the increase in viscosity. However, if DNA undergoes groove mode of binding with

compound, kink or bend in the DNA helix is produced that results in the decrease of DNA length and hence the viscosity either decreases or remain unaffected [48]. Figure 5 describes the effect of increasing concentration ratio of compound-DNA upon the relative viscosity of the DNA. It can be clearly evidenced from the figure that during the compound-DNA adduct formation the viscosity of the DNA increased showing intercalative mode of binding. The viscosity results completely support the UV-Vis absorption findings discussed in section 3.3.

Figure 5

3.5. Structural analysis DNA binding by molecular docking

Molecular docking is a simulation technique used to express the "best-fit" binding orientation of a compound under study with a specific macromolecule like DNA. It further describes the anticipated structure of intermolecular complex system formed by the interaction of two or more molecules [27]. DNA can bind to a compound *via* different possible mutual conformations and are commonly referred as its binding modes [49]. In order to support our experimental results of compound-DNA binding docking simulations were performed.

Pose view analysis of best and stable conformations the compounds **1** and **2** (Figure 6a and 6c) and showed that both compounds interacted with *via* intercalation binding mode between stacked base pairs of double helical DNA. An acute looks over 2D ligplot (Figure 6b and 6d) depicted that compound **2** developed four hydrogen bonds i.e., one between H-atom of hydroxyl group and N-atom of adenine (DA-A6), second and third hydrogen bond between H atom of -OH on compound **2** with N-atom of another adenine (DA-A5), fourth hydrogen bond between H-atom of hydroxyl group and O-atom of guanine (DG-A3). Compound **1** intercalated via three hydrogen bonds; one hydrogen bond is formed between H-atom of hydroxyl group on compound **1** and O- atom of guanine (DG-A3), second bond was developed between H-atom of hydroxyl group and O-atom of guanine DG (A4), third hydrogen bond was constructed between O-atom of hydroxyl on compound **1** and H-atom of guanine DG (A3).Greater number of hydrogen bonds in compound **2** contributed to its greater binding strength with 1D66 (Table 5).

Several electronic and steric descriptors for compound **1** and **2** were calculated (Table 6) respectively. E_{HOMO} and E_{LUMO} that describes electron donating and accepting character of a compound also determine the energetic dependency of binding a compound with macromolecules. A compound will be considered as electron-donating if the E_{HOMO} value increase whereas it will be considered as electron-accepting its E_{LUMO} value decreases [31].

Steric parameters for docked conformation i.e., partition coefficient (log P) and Molar refractivity (M_R) were also calculated and they exhibited inverse correlation with binding constant K_b (Table 6). SlogP is illustrative of steric interactions and hydrophobicity of the molecule while M_R gives extent of polarizability of a small molecule. Both of these descriptors exhibited converse correlation with binding strength (K_b) of the compound **1** and **2**. Hydrophobic surface area (V_{surf}) is considered as another important steric descriptor calculated which revealed greater value of V_{surf} for compound **2,** therefore greater overlapping of compound **2** with electron rich DNA resulted in its higher K_b with 1D66.

Figure 6

Tables 5-6

3.6. DPPH scavenging activity

The stable DPPH free radical scavenging model has been widely applied to efficiently determine the antioxidant activities. The potential antioxidant activity of compounds **1** and **2** were evaluated by DPPH radical-scavenging assay, whereby DPPH free radicals were applied in the rapid analysis of the antioxidants, and while scavenging these radicals, the antioxidants donate hydrogen and a stable 1, 1-diphenyl-2-picrylhydrazine (DPPH-H) molecule is formed. The DPPH radical generally gives a strong absorption band at 517 nm due to extensive delocalization of free electron [50]. However, this band disappears due to non-availability of free electron by abstracting hydrogen radical from the interacting compound [51]. The variation produced is a key factor that defines the antioxidant potential of tested compound. Both compounds were tested for their potential antioxidant activities by the interaction of fixed concentration of DPPH solution with varying concentrations of compound **1** and **2** The percentage inhibition was calculated by using the Eq.

% Inhibition of DPPH = A_o – As / A_o× 100

Where A_o and As in equation are the absorbance of DPPH in the absence and presence of the test compound, respectively.

The inhibition of DPPH by the tested compounds in contrast to ascorbic acid (standard antioxidant) has been shown in Figure 7. The plot between percentage inhibition and concentration clearly shows that with increase in the concentration of tested compounds, percentage inhibition increases, where maximum inhibition of DPPH free radical was observed at a concentration of about 52 µg/mL. The test compounds have scavenging activity of 36 % to

52 % for **1** and 38% to 54% for **2** within the investigated range due to the donation of H from OH group and a stable DPPH-H molecule was formed. In compound **1** the most probable chances of H atom abstraction is from the OH group attached to C-1 as the H of the other OH attached to C-5 of aromatic ring is involved in strong intramolecular H-bonding with N atom resulting in the formation of stable 6-membered ring. While in compound **2** there are total 3 OH groups in which one is involved in intramolecular H-bonding with N atom (the one attached to C-5 of aromatic ring) while the other two (one attached to C-1 and other attached to C-6 of aromatic ring) may influence the anti-oxidant activity. Also the anti-oxidant activity of compound **2** is slightly higher than that of compound **1**.

Figure 7

3.7. Computational structure analysis by DFT studies

The geometries of synthesized compounds were optimized by B3LYP method of DFT with default convergence criteria and without any constraints. DFT considers electronic structure of a molecule for theoretical investigations through a quantum mechanical approach. The various parameters like maximum charge distribution, HOMO-LUMO energy gap and energies, dipole moment, ionization potential, electronegativity, electron affinity, global hardness and UV-visible analysis were calculated from the optimized geometry. For understanding the electronic structures of our compounds and its possibilities of interaction with different biological macromolecules like DNA these theoretical results interpretation are helpful. B3LYP Global hybrid [52] method was selected for the calculation purposes in order to get accurate non-bonding interactions that are responsible for crystal structure stability. From the calculations of optimized structure it can be concluded that both compounds have planar geometry which favors intercalation mode. The calculated bond angles and lengths (Table 7) correlated well with the experimental data obtained by single crystal X-ray diffraction analysis. However, slight deviations observed can be explained on the basis of the fact that DFT calculations used isolated molecules in gaseous phase while the single crystal X-ray analysis was performed on the solid phase of the compounds [53].

Table 7

3.7.1. Frontier molecular orbital (FMO) analysis

Pictorial representation of the charge distributions on the optimized molecule geometry and HOMO-LUMO orbitals are shown in Figure S7 of the supplementary data, while different

computational parameters of the optimized molecule are given in Table 9. The optimized structures of both compounds **1** and **2** have shown planner geometry; so, probably both compounds interact with DNA base pairs *via* intercalative mode of interaction. Furthermore, oxygen atom of hydroxyl group (OH) has high electron density, so it has the probability to form a hydrogen bond with DNA base pairs. While the hydrogen atom of OH group is electron deficient, so it has the tendency to form a hydrogen bond by accepting an electron pair from DNA base pairs.

Parameters like molecule softness/hardness, chemical reactivity and stability can be evaluated with the HOMOs and LUMOs which are also known as frontier molecular orbitals (FMOs) [54]. Ionization potential and electron affinity has a direct dependence on the energies of FMOs as these are the electron donating and accepting orbitals of a molecule. Importantly the difference in energy between HOMO and LUMO depicts the energy gap and hence can affect the chemical reactivity of the compound. Lower the energy gap between HOMO and LUMO, more the compound will be reactive or in other words less stable [52, 55, 56]. Difference in energy of HOMO and LUMO decides the softness/hardness of the compound. When the energy difference is higher it shows more hardness in the respective compound and vice versa. For both compounds, the calculated HOMO and LUMO energy, energy gap, ionization potential, electron affinity (A), electronic chemical potential (μ), electronegativity (χ), molecular softness (S) and hardness (η), and electrophilicity index (ω) are given in the Table 8**.** The calculated energy gap, and smaller value of hardness, while higher value of dipole moment depicted the reactive nature of both compounds [57]. In addition, electronic absorption spectra for compounds **1** and **2** in gas phase were calculated using the Time-Dependent Self Consistent Field (TD- SCF) method by using the optimized structure in ethanol as solvent with the same level of theory. The simulated UV-visible absorption maxima (λ_{max}) values, theoretical electronic excitation energies and oscillator strengths are depicted in Table S2. As can be clear from Table S2, the simulated absorption maxima values for the compounds **1** and **2** are found to be 302.71 and 306.53 nm, respectively. The oscillator strength *f* has no dimension and tells about the strength of an electronic transition. The maximum absorption at 302.71 (compound **1**) and 306.53 (compound **2**) nm, respectively is assigned to the transition from HOMO to LUMO molecular orbital.

Table 8

3.8. CTAB-complex interaction study

Surfactant can be possibly used as a drug carriers because of its potential behavior of establishing soluble environment even for very poorly soluble drugs, and hence increases the bioavailability together with reducing the hostile effect of the drugs [58]. Each surfactant form micelles at different concentrations called its CMC value, which changes by the interaction of surfactant with drugs. Now when a drug is administered with a surfactant, the CMC value either increases representing good bioavailability of drug upon dilution or it decreases/remains constant representing low bioavailability of drug.

Herein, we studied the CTAB-compounds interactions *via* conductometric method. In order to emphasize the CTAB-compound study through their specific conductance, 1 mM solutions of compound **1** and **2** were prepared in methanol and interacted with varying concentration of CTAB i.e. ranging from 0 to 7 mM. Initially the specific conductance of compound solutions increases with increase in CTAB concentration till a point called as inflection point was observed and hereafter CTAB monomers tend to form micelle and the conductance is mainly due to free Br^- ions (Figure 8) [59]. Generally free ions ($CTAB^+$ and Br^-) formed in the solution are responsible for the sharp increase in conductance in the pre-micellar concentration region while comparative decrease in the increase rate of conductance in post-micellar region is because of the micelle formation from the available free ions. However, on interaction of compound molecules, the repulsion between the positive charges of N atom of $CTAB^+$ monomers decreases by reducing its charge density hence increases the CMC value.

For compound **1** while interacting with CTAB system CMC value is found to be 0.003M whereas the value is 0.0031M when compound **2** interacts with CTAB (Figure 8). CMC value for compounds-CTAB system is comparatively higher than the reported free CTAB value (0.0009 M) [60]. This increase in CMC value indicates strong interaction of compounds with the surfactant (CTAB) that might results in higher bioavailability of the compounds in biological system.

Gibbs free energy of micellization (ΔGm) was calculated using the equation:

$\Delta Gm = 2.303(1+\beta)\ RT\log X_{cmc}$

$\beta = 1-\alpha$ (β = degree of the counter ion binding)

$\alpha = S_2/S_1$(α = degree of dissociation or ionization, calculated before and after CMC from the ratio of plots)

S_1 and S_2 are slopes of conductivity–concentration plots before and after CMC. It is taken in mole fractions called as Xcmc which in aqueous solution can be calculated as:

X_{cmc} = cmc/55.55

For compound **1** and **2** ΔGm value is found to be -36 kJ mol^{-1} and -34 kJ mol^{-1}, respectively, where its negative value indicates spontaneous solubilization of the compounds in surfactant micelles system.

Figure 8

3.9. *In vitro* antibacterial activity

The agar well diffusion method was used to carry out the in vitro antibacterial activity against five different bacterial strains: *C. Staphylococci, MRSA, S. Aureus, E. Coli* and *K. Pneumoniae*. The zone inhibition (mm) of both the compounds was measured against their activity (Table 10). Both compounds showed good anti-bacterial activity and is comparable to that of standard. The anti-bacterial activity was higher against G+ve (*S. aureus*) bacteria than against G -ve bacteria. The antibacterial activity and inhibition zone around the tested compounds can be caused by their bactericide effects or their bacteriostatic effects [25].

Table 10

3.10. *In vitro* antifungal activity

The agar well diffusion protocol was used to carry out the antifungal activity against four different strains of fungi and is summarized in Table 10. Terbinafine and DMSO were used as positive and negative controls, respectively. The zone of inhibition for both compounds was measured as a function of their activity. Percentage inhibition value was evaluated by following formula:

$$\text{Percent inhibition of fungal growth} = \left[\frac{\text{Growth diameter in test compound (mm)}}{\text{Growth diameter in control (mm)}}\right] \times 100$$

Compound **1** has shown maximum inhibition of 79% against *M. species* fungal strain while compound **2** has shown maximum inhibition of 69% against *A. niger*. Overall both the compounds have shown good inhibition against all the tested fungal strains.

Table 10

Conclusions

The titled Schiff bases derived from 2,3-dihyroxybenzaldehyde (**1**) and *o*-vanillin (**2**) were synthesized and characterized by various analytical techniques. Crystallographic data of the

investigated compounds show that both the compounds crystallized in the monoclinic crystal system with space group C2/c and exhibited strong intramolecular N–H···O hydrogen bond resulting in the formation of stable 6-membered ring. The geometric parameters obtained from DFT studies and spectroscopic properties obtained from experimental data showed excellent correlation with each others. The interaction of the titled compounds with DNA was investigated by UV-visible spectroscopy and viscometry showing the intercalative mode of interaction. Moreover, the interaction of the compounds with CTAB is characterized by higher CMC and negative ΔG values which indicates good bioavailability and spontaneous solubilization of compounds. The antibacterial and antifungal evaluation of compounds exhibit relatively good results as compared to standard drugs, cefixime and terbinafine, respectively.

Acknowledgement

S. Ali is thankful to Quaid-i-Azam University Islamabad Pakistan for financial support (URF 2019).

References

[1] M. Andruh, The exceptionally rich coordination chemistry generated by Schiff-base ligands derived from o-vanillin, Dalton Transactions 44(38) (2015) 16633-16653.
[2] K. Dhahagani, M.P. Kesavan, K.G.G. Vinoth, L. Ravi, G. Rajagopal, J. Rajesh, Crystal structure, optical properties, DFT analysis of new morpholine based Schiff base ligands and their copper (II) complexes: DNA, protein docking analyses, antibacterial study and anticancer evaluation, Materials Science and Engineering: C 90 (2018) 119-130.
[3] M. Rajasekar, S. Sreedaran, R. Prabu, V. Narayanan, R. Jegadeesh, N. Raaman, A. Kalilur Rahiman, Synthesis, characterization, and antimicrobial activities of nickel (II) and copper (II) Schiff-base complexes, Journal of Coordination Chemistry 63(1) (2010) 136-146.
[4] T. Jeewoth, H. Li Kam Wah, M.G. Bhowon, D. Ghoorohoo, K. Babooram, Synthesis and anti-bacterial/catalytic properties of Schiff bases and Schiff base metal complexes derived from 2, 3-diaminopyridine, Sythesis and Reactivity in Inorganic and Matel-Organic Chemistry 30(6) (2000) 1023-1038.
[5] N. Dharmaraj, P. Viswanathamurthi, K. Natarajan, Ruthenium (II) complexes containing bidentate Schiff bases and their antifungal activity, Transition Metal Chemistry 26(1-2) (2001) 105-109.
[6] J.-P. Costes, F. Dahan, F. Nicodeme, A trinuclear gadolinium complex: structure and magnetic properties, Inorganic chemistry 40(20) (2001) 5285-5287.
[7] J. Tang, I. Hewitt, N. Madhu, G. Chastanet, W. Wernsdorfer, C.E. Anson, C. Benelli, R. Sessoli, A.K. Powell, Dysprosium triangles showing single-molecule magnet behavior of thermally excited spin states, Angewandte Chemie International Edition 45(11) (2006) 1729-1733.
[8] J. Luzon, K. Bernot, I.J. Hewitt, C.E. Anson, A.K. Powell, R. Sessoli, Spin chirality in a molecular dysprosium triangle: the archetype of the noncollinear Ising model, Physical review letters 100(24) (2008) 247205.
[9] L.F. Chibotaru, L. Ungur, A. Soncini, The origin of nonmagnetic Kramers doublets in the ground state of dysprosium triangles: evidence for a toroidal magnetic moment, Angewandte Chemie 120(22) (2008) 4194-4197.

[10] X. Liu, C. Manzur, N. Novoa, S. Celedón, D. Carrillo, J.-R. Hamon, Multidentate unsymmetrically-substituted Schiff bases and their metal complexes: Synthesis, functional materials properties, and applications to catalysis, Coordination Chemistry Reviews 357 (2018) 144-172.
[11] F. Cuenú, J. Londoño-Salazar, J.E. Torres, R. Abonia, R.F. D'Vries, Synthesis, structural characterization and theoretical studies of a new Schiff base 4-(((3-(tert-Butyl)-(1-phenyl) pyrazol-5-yl) imino) methyl) phenol, Journal of Molecular Structure 1152 (2018) 163-176.
[12] J. Gauss, Calculation of NMR chemical shifts at second-order many-body perturbation theory using gauge-including atomic orbitals, Chemical physics letters 191(6) (1992) 614-620.
[13] J. Gauss, Effects of electron correlation in the calculation of nuclear magnetic resonance chemical shifts, The Journal of chemical physics 99(5) (1993) 3629-3643.
[14] J. Gauss, Accurate calculation of NMR chemical shifts, Berichte der Bunsengesellschaft für physikalische Chemie 99(8) (1995) 1001-1008.
[15] A.M. Mendoza-Wilson, D. Glossman-Mitnik, CHIH-DFT study of the electronic properties and chemical reactivity of quercetin, Journal of Molecular Structure: THEOCHEM 716(1-3) (2005) 67-72.
[16] O.F. Vázquez-Vuelvas, J.V. Hernández-Madrigal, R. Gaviño, M.A. Tlenkopatchev, D. Morales-Morales, J.M. Germán-Acacio, Z. Gomez-Sandoval, C. Garcias-Morales, A. Ariza-Castolo, A. Pineda-Contreras, X-ray, DFT, FTIR and NMR structural study of 2, 3-dihydro-2-(R-phenylacylidene)-1, 3, 3-trimethyl-1H-indole, Journal of Molecular Structure 987(1) (2011) 106-118.
[17] G.-X. Tan, X.-C. Liu, (E)-2-[(2-Hydroxyethyl) iminiomethyl]-6-methoxyphenolate, Acta Crystallographica Section E: Structure Reports Online 65(3) (2009) o559-o559.
[18] W.L. Armarego, C. Chai, Purification of laboratory chemicals, Butterworth-Heinemann2013.
[19] G.M. Sheldrick, SHELXT–Integrated space-group and crystal-structure determination, Acta Crystallographica Section A: Foundations and Advances 71(1) (2015) 3-8.
[20] S. Dey, S. Sarkar, H. Paul, E. Zangrando, P. Chattopadhyay, Copper (II) complex with tridentate N donor ligand: synthesis, crystal structure, reactivity and DNA binding study, Polyhedron 29(6) (2010) 1583-1587.
[21] A. Munir, M. Sirajuddin, M. Zubair, A. Haider, S. Tirmizi, S. Ali, H. Khan, K. Ullah, I. Aziz, Synthesis, spectroscopic characterization, and biological screening of levofloxacin based organotin (IV) derivatives, Russian Journal of General Chemistry 87(10) (2017) 2380-2390.
[22] M. Sirajuddin, S. Ali, V. McKee, N. Akhtar, S. Andleeb, A. Wadood, Spectroscopic characterizations, structural peculiarities, molecular docking study and evaluation of biological potential of newly designed organotin (IV) carboxylates, Journal of Photochemistry and Photobiology B: Biology (2019) 111516.
[23] M. Sirajuddin, S. Ali, M.N. Tahir, Pharmacological investigation of mono-, di-and tri-organotin (IV) derivatives of carbodithioates: Design, spectroscopic characterization, interaction with SS-DNA and POM analyses, Inorganica Chimica Acta 439 (2016) 145-158.
[24] S. Satyanarayana, J.C. Dabrowiak, J.B. Chaires, Tris (phenanthroline) ruthenium (II) enantiomer interactions with DNA: mode and specificity of binding, Biochemistry 32(10) (1993) 2573-2584.
[25] M. Sirajuddin, V. McKee, M. Tariq, S. Ali, Newly designed organotin (IV) carboxylates with peptide linkage: Synthesis, structural elucidation, physicochemical characterizations and pharmacological investigations, European journal of medicinal chemistry 143 (2018) 1903-1918.
[26] S. Chatzieleftheriou, S. Anogiannakis, D.N. Theodorou, N.D. Lagaros, SimNano: A Trust Region Strategy for Large-Scale Molecular Systems Energy Minimization Based on Exact Second-Order Derivative Information, Journal of Chemical Information and Modeling 59(1) (2019) 190-205.
[27] B.A. Arthington-Skaggs, M. Motley, D.W. Warnock, C.J. Morrison, Comparative evaluation of PASCO and national committee for clinical laboratory standards M27-A broth microdilution methods for antifungal drug susceptibility testing of yeasts, Journal of clinical microbiology 38(6) (2000) 2254-2260.

[28] Y. Li, Z.-Y. Yang, Z.-C. Liao, Z.-C. Han, Z.-C. Liu, Synthesis, crystal structure, DNA binding properties and antioxidant activities of transition metal complexes with 3-carbaldehyde-chromone semicarbazone, Inorganic Chemistry Communications 13(10) (2010) 1213-1216.
[29] P.A. Onocha, G.K. Oloyede, O.A. Bamkole, UV-visible investigation of antioxidant and toxicity activities of methanolic fractions of Acalypha hispida (Burn. f) leaves, European Journal of Scientific Research 49(3) (2011) 322-331.
[30] G.K. Oloyede, P.A. Onocha, B.B. Olaniran, Phytochemical, toxicity, antimicrobial and antioxidant screening of leaf extracts of Peperomia pellucida from Nigeria, Advances in Environmental Biology 5(12) (2011) 3700-3709.
[31] M.N. Zafar, F. Perveen, M.F. Nazar, E.U. Mughal, H. Rafique, M.N. Tahir, M.S. Akbar, S. Zahra, Synthesis, characterization, DNA-Binding, enzyme inhibition and antioxidant studies of new N-methylated derivatives of pyridinium amine, Journal of Molecular Structure 1137 (2017) 84-96.
[32] M. Frisch, G. Trucks, H.B. Schlegel, G.E. Scuseria, M.A. Robb, J.R. Cheeseman, G. Scalmani, V. Barone, B. Mennucci, G. Petersson, Gaussian 09, revision a. 02, gaussian, Inc., Wallingford, CT 200 (2009).
[33] M.J. Frisch, G. Trucks, H.B. Schlegel, G. Scuseria, M. Robb, J. Cheeseman, G. Scalmani, V. Barone, B. Mennucci, G. Petersson, Gaussian 09, revision A. 1, Gaussian Inc. Wallingford CT 27 (2009) 34.
[34] A. Frisch, H. Hratchian, R. Dennington II, T. Keith, J. Millam, B. Nielsen, A. Holder, J. Hiscocks, GaussView Version 5.0. 8, Gaussian, Inc., Wallingford, CT (2009).
[35] S. Dhanavel, N. Manivannan, N. Mathivanan, V.K. Gupta, V. Narayanan, A. Stephen, Preparation and characterization of cross-linked chitosan/palladium nanocomposites for catalytic and antibacterial activity, Journal of Molecular Liquids 257 (2018) 32-41.
[36] M. Khatami, I. Sharifi, M.A. Nobre, N. Zafarnia, M.R. Aflatoonian, Waste-grass-mediated green synthesis of silver nanoparticles and evaluation of their anticancer, antifungal and antibacterial activity, Green Chemistry Letters and Reviews 11(2) (2018) 125-134.
[37] S.H.M. Mehr, K. Fukuyama, S. Bishop, F. Lelj, M.J. MacLachlan, Deuteration of Aromatic Rings under Very Mild Conditions through Keto-Enamine Tautomeric Amplification, The Journal of organic chemistry 80(10) (2015) 5144-5150.
[38] P. Tyagi, M. Tyagi, S. Agrawal, S. Chandra, H. Ojha, M. Pathak, Synthesis, characterization of 1, 2, 4-triazole Schiff base derived 3d-metal complexes: Induces cytotoxicity in HepG2, MCF-7 cell line, BSA binding fluorescence and DFT study, Spectrochimica Acta Part A: Molecular and Biomolecular Spectroscopy 171 (2017) 246-257.
[39] Z. Popović, V. Roje, G. Pavlović, D. Matković-Čalogović, G. Giester, The first example of coexistence of the ketoamino–enolimino forms of diamine Schiff base naphthaldimine parts: the crystal and molecular structure of N, N′-bis (1-naphthaldimine)-o-phenylenediamine chloroform (1/1) solvate at 200 K, Journal of Molecular Structure 597(1) (2001) 39-47.
[40] F.H. Allen, O. Kennard, D.G. Watson, L. Brammer, A.G. Orpen, R. Taylor, Tables of bond lengths determined by X-ray and neutron diffraction. Part 1. Bond lengths in organic compounds. Journal of the Chemical Society, Perkin Transactions, 2 12 (1987) S1-S19.
[41] Y.X. Sun, R. Zhang, L.J. Tian, L. X. Xu, S.L. Sun, Acta Cryst. E62 (2006) o4433–o4435.
[42] S. W. Ng,. Acta Cryst. E64 (2008) o2455.
[43] A. Pyle, J. Rehmann, R. Meshoyrer, C. Kumar, N. Turro, J.K. Barton, Mixed-ligand complexes of ruthenium (II): factors governing binding to DNA, Journal of the American Chemical Society 111(8) (1989) 3051-3058.
[44] M. Sirajuddin, S. Ali, A. Badshah, Drug–DNA interactions and their study by UV–Visible, fluorescence spectroscopies and cyclic voltametry, Journal of Photochemistry and Photobiology B: Biology 124 (2013) 1-19.

[45] K. Ullah, M. Sirajuddin, M. Zubair, A. Haider, S. Ali, F. Ullah, G. Dutkiewicz, M. Kubicki, C. Rizzoli, Designing of homo and heteroleptic zinc (II) carboxylates: synthesis, spectroscopic characterizations, DNA binding study, CTAB interaction and in vitro antimicrobial evaluations, Journal of the Iranian Chemical Society (2019) 1-15.
[46] K.A. Fletcher, S. Pandey, Surfactant aggregation within room-temperature ionic liquid 1-ethyl-3-methylimidazolium bis (trifluoromethylsulfonyl) imide, Langmuir 20(1) (2004) 33-36.
[47] N. Revathi, M. Sankarganesh, J. Rajesh, J.D. Raja, Biologically active Cu (II), Co (II), Ni (II) and Zn (II) complexes of pyrimidine derivative Schiff base: DNA binding, antioxidant, antibacterial and in vitro anticancer studies, Journal of Fluorescence 27(5) (2017) 1801-1814.
[48] D.-D. Li, J.-L. Tian, W. Gu, X. Liu, S.-P. Yan, A novel 1, 2, 4-triazole-based copper (II) complex: Synthesis, characterization, magnetic property and nuclease activity, Journal of Inorganic Biochemistry 104(2) (2010) 171-179.
[49] N. Sharma, K. Jha, Molecular docking: an overview, J. Adv. Sci. Res 1(1) (2010) 67-72.
[50] M. Zamani, A.M. Delfani, M. Jabbari, Scavenging performance and antioxidant activity of γ-alumina nanoparticles towards DPPH free radical: Spectroscopic and DFT-D studies, Spectrochimica Acta Part A: Molecular and Biomolecular Spectroscopy 201 (2018) 288-299.
[51] A. Bhogale, N. Patel, P. Sarpotdar, J. Mariam, P. Dongre, A. Miotello, D. Kothari, Systematic investigation on the interaction of bovine serum albumin with ZnO nanoparticles using fluorescence spectroscopy, Colloids and Surfaces B: Biointerfaces 102 (2013) 257-264.
[52] Z. Messasma, A. Ourari, R. Mahdadi, S. Houchi, D. Aggoun, A. Kherbache, E. Bentouhami, Synthesis, spectral characterization, DFT computational studies and inhibitory activity of novel N 2 S 2 tetradentates Schiff bases on metallo-beta-lactamases of Acinetobacter baumannii, Journal of Molecular Structure 1171 (2018) 672-681.
[53] S.Y. Ebrahimipour, M. Khosravan, J. White, S. Fekri, Preparation, crystal structure, spectroscopic studies, DFT calculations, antibacterial activities and molecular docking of a tridentate Schiff base ligand and its cis-MoO2 complex, Applied Organometallic Chemistry 32(4) (2018) e4233.
[54] S. Abbas, H.H. Nasir, S. Zaib, S. Ali, T. Mahmood, K. Ayub, M.N. Tahir, J. Iqbal, Carbonic anhydrase inhibition of Schiff base derivative of imino-methyl-naphthalen-2-ol: Synthesis, structure elucidation, molecular docking, dynamic simulation and density functional theory calculations, Journal of Molecular Structure 1156 (2018) 193-200.
[55] G.-D. Tang, J.-Y. Zhao, R.-Q. Li, Z.-C. Zhang, Synthesis, characteristic and theoretical investigation of the structure, electronic properties and second-order nonlinearity of salicylaldehyde Schiff base and their derivatives, Spectrochimica Acta Part A: Molecular and Biomolecular Spectroscopy 78(1) (2011) 449-457.
[56] R.M. Ramadan, A.K.A. Al-Nasr, O.A. Ali, Synthesis, spectroscopic, DFT studies and biological activity of some ruthenium carbonyl derivatives of bis-(salicylaldehyde) phenylenediimine Schiff base ligand, Journal of Molecular Structure 1161 (2018) 100-107.
[57] G. Elmacı, H. Duyar, B. Aydıner, N. Seferoğlu, M.A. Naziri, E. Şahin, Z. Seferoğlu, The syntheses, molecular structure analyses and DFT studies on new benzil monohydrazone based Schiff bases, Journal of Molecular Structure 1162 (2018) 37-44.
[58] G.P. Kumar, P. Rajeshwarrao, Nonionic surfactant vesicular systems for effective drug delivery—an overview, Acta Pharmaceutica Sinica B 1(4) (2011) 208-219.
[59] M. Zubair, M. Sirajuddin, A. Haider, K. Ullah, I. Ullah, A. Munir, S. Ali, M.N. Tahir, Synthesis, physicochemical characterizations and in vitro biological evaluations of amide based Zn (II) carboxylates, Inorganica Chimica Acta 482 (2018) 567-578.
[60] W. Li, M. Zhang, J. Zhang, Y. Han, Self-assembly of cetyl trimethylammonium bromide in ethanol-water mixtures, Frontiers of Chemistry in China 1(4) (2006) 438-442.

Table 1: Crystal data and structure refinement parameters for compound **1** and **2**

Parameters	**Compound 1**	**Compound 2**
Formula/molecular weight	$C_{10}H_{13}NO_3$/195.21	$C_9H_{11}NO_3$/181.19
Temperature/K	296(2)	296(2)
Crystal system/Space group	Monoclinic/C2/c	Monoclinic/C2/c
a, b, c/Å	24.618(4), 5.0167(7), 31.985(5)	17.118(3),7.3373(10), 15.989(2)
α, β, γ /°	90, 101.612(6), 90	90, 116.472(7), 90
V/Å^3	3869.3(11)	1797.7(5)
Z	16	8
ρ_{calc}g/cm^3	1.340	1.339
μ/mm^{-1}	0.099	0.101
F(000)	1664.0	768.0
Crystal dimension/mm^3	0.39 × 0.22 × 0.20	0.42 × 0.32 × 0.28
Radiation	MoKα (λ = 0.71073)	MoKα (λ = 0.71073)
2θ range for data collection/°	4.66 to 52	5.316 to 51.972
Index ranges	-29 ≤ h ≤ 30, -6 ≤ k ≤ 5, -30 ≤ l ≤ 39	-14 ≤ h ≤ 20, -8 ≤ k ≤ 9, -19 ≤ l ≤ 17
Reflections collected	11702	5028
Independent reflections	3802 [R_{int} = 0.0493, R_{sigma} = 0.0647]	1760 [R_{int} = 0.0517, R_{sigma} = 0.0620]
Data/restraints/parameters	3802/0/257	1760/0/120
S on F^2	1.039	1.032
Final R indexes [I>=2σ (I)]	R_1 = 0.0538, wR_2 = 0.1410	R_1 = 0.0494, wR_2 = 0.1318
Final R indexes [all data]	R_1 = 0.0899, wR_2 = 0.1606	R_1 = 0.0661, wR_2 = 0.1479
Largest diff. peak/hole / e Å^{-3}	0.41/-0.30	0.22/-0.19
CCDC#	1888257	1888256

Table 2: Selected bond lengths (Å) for Compounds **1** and **2**

Compound 1			
Atom-Atom	**Length/Å**	**Atom-Atom**	**Length/Å**
O1-C1	1.280(3)	O4-C11	1.354(3)
O2-C2	1.367(3)	O5-C12	1.365(3)
O2-C7	1.425(3)	O5-C17	1.426(3)
O3-C10	1.417(3)	O6-C20	1.415(3)
N1-C8	1.292(3)	N2-C18	1.254(3)
N1-C9	1.463(3)	N2-C19	1.468(3)
C1-C6	1.433(3)	C11-C16	1.393(3)
C1-C2	1.446(3)	C11-C12	1.411(3)
C2-C3	1.364(3)	C12-C13	1.375(3)
C3-C4	1.405(4)	C13-C14	1.384(4)
C4-C5	1.354(3)	C14-C15	1.375(4)
C5-C6	1.423(4)	C15-C16	1.405(4)
C6-C8	1.412(3)	C16-C18	1.460(3)
C9-C10	1.514(3)	C19-C20	1.487(4)
Compound 2			
O1-C1	1.3001(18)	C2-C3	1.368(2)
O2-C2	1.367(2)	C3-C4	1.406(3)
O3-C9	1.401(2)	C4-C5	1.352(3)
N1-C7	1.289(2)	C5-C6	1.422(2)
N1-C8	1.457(2)	C6-C7	1.416(2)
C1-C2	1.427(2)	C8-C9	1.510(3)
C1-C6	1.430(2)		

Table 3: Selected bond angles (˚) for compounds **1** and **2**

Compound 1			
Atom-Atom-Atom	**Angle/˚**	**Atom-Atom-Atom**	**Angle/˚**
C2-O2-C7	117.4(2)	C12-O5-C17	117.2(2)
C8-N1-C9	125.0(2)	C18-N2-C19	119.3(3)
O1-C1-C6	122.4(2)	O4-C11-C16	122.7(2)
O1-C1-C2	121.6(2)	O4-C11-C12	117.8(2)
C6-C1-C2	116.0(2)	C16-C11-C12	119.5(2)
C3-C2-O2	125.5(2)	O5-C12-C13	125.9(2)
C3-C2-C1	121.1(2)	O5-C12-C11	114.6(2)
O2-C2-C1	113.4(2)	C13-C12-C11	119.5(2)
C2-C3-C4	121.6(2)	C12-C13-C14	120.8(2)
C5-C4-C3	119.9(2)	C15-C14-C13	120.4(2)
C4-C5-C6	120.7(2)	C14-C15-C16	119.9(3)
C8-C6-C5	119.1(2)	C11-C16-C15	119.8(2)
N1-C8-C6	124.7(2)	N2-C18-C16	122.8(3)
N1-C9-C10	112.04(18)	N2-C19-C20	113.4(2)
O3-C10-C9	112.90(19)	O6-C20-C19	111.6(2)
Compound 2			
C7-N1-C8	124.40(15)	C5- C4-C3	119.56(17)
O1-C1-C2	120.62(14)	C4- C5-C6	121.15(17)
O1-C1-C6	122.79(14)	C7- C6-C5	119.25(16)
C2-C1-C6	116.58(14)	C7- C6-C1	120.65(15)
O2-C2-C3	119.53(15)	C5- C6-C1	120.10(16)
O2-C2-C1	119.07(14)	N1- C7-C6	125.14(16)
C3-C2-C1	121.40(15)	N1- C8-C9	111.51(15)

C2-C3-C4	121.20(16)	O3- C9-C8	108.42(15)

Table 4: Hydrogen-bond lengths and bond angles (Å,˚) for compounds **1** and **2**

D-H···A	**d(D-H)/Å**	**d(H-A)/Å**	**d(D-A)/Å**	**D-H-A/°**
Compound 1				
O3-H3A···O1[1]	0.82	1.91	2.722(2)	169.8
N1-H1···O1	0.86	1.96	2.630(2)	134.2
N1-H1···O1[1]	0.86	2.59	3.108(3)	119.9
C8-H8···O4	0.93	2.56	3.450(3)	160.7
C9-H9B···O1[1]	0.97	2.65	3.132(3)	110.7
O6-H6···O3[2]	0.82	2.10	2.875(2)	156.6
N2-H2···O4	0.86	1.96	2.630(3)	133.3
Compound 2				
O2-H2··· O1	0.82	2.33	2.7543(16)	112.7
O2- H2··· O1[1]	0.82	2.02	2.7304(17)	144.0
O3- H3A··· O1[2]	0.82	1.92	2.7336(18)	170.0
N1- H1··· O1	0.86	2.00	2.6658(17)	133.5
C7- H7··· O3[3]	0.93	2.46	3.361(2)	162.0
C8- H8B··· O2[4]	0.97	2.65	3.591(3)	163.0

Symmetry transformations used to generate equivalent atoms in compound 1: (1) 1/2-X,1/2-Y,-Z; (2) -1/2+X,1/2+Y,+Z

Symmetry transformations used to generate equivalent atoms in compound 2: (1) 1/2-X,-1/2-Y,1-Z; (2) -X,-Y,1-Z; (3) -X,1-Y,1-Z; (4) +X,-Y,1/2+Z

Table 5: Binding constant (K_b), Gibbs free energies (ΔG) and electronic descriptors of compounds **1** and **2** calculated from molecular docking analysis

Binding Parameter	**Compound 1**	**Compound 2**
K_b (M^{-1})	6.5×10^{1}	9.92×10^{2}
ΔG ($kJmol^{-1}$)	-10.37	-17.05

Table 6: Electronic descriptors of compounds **1** and **2** calculated from molecular docking analysis

Comp. #	**Electronic descriptors**					
	E_{HOMO} (kJ mol^{-1})	E_{LUMO} (kJ mol^{-1})	E_{IP} (kJ mol^{-1})	E_{ele} (kJ mol^{-1})	E_{vander} (kJ mol^{-1})	E_{tot} (kJ mol^{-1})
1	-37.18	-2.60	37.18	-1166828.69	0.00	-2198895.92
2	-40.02	-2.79	2.36	-1228896.86	0.00	-238328254.88

Steric descriptors				
Comp. #	H_f	SlogP	M_R	V_{surf}
1	-99.630	0.6940	5.4354	194.8
2	-98.547	0.5090	4.9318	195.6

Table 7: Comparison of experimental and simulated geometric parameters of compounds **1** and **2**

Bond lengths (Å)			**Bond angles (°)**		
Parameters	**Experimental**	**Calculated**	**Parameters**	**Experimental**	**Calculated**
Compound 1					
O1-C1	1.280(3)	1.283	C2-O2-C7	117.4(2)	117.6
O2-C2	1.367(3)	1.371	C8-N1-C9	125.0(2)	125.4
O2-C7	1.425(3)	1.417	O1-C1-C6	122.4(2)	122.8
O3-C10	1.417(3)	1.434	O1-C1-C2	121.6(2)	121.9
N1-C8	1.292(3)	1.280	C6-C1-C2	116.0(2)	116.4
N1-C9	1.463(3)	1.447	C3-C2-O2	125.5(2)	125.1
O4-C11	1.354(3)	1.345	C12-O5-C17	117.2(2)	117.4
O5-C12	1.365(3)	1.342	C18-N2-C19	119.3(3)	119.5
O5-C17	1.426(3)	1.432	O4-C11-C16	122.7(2)	122.9
O6-C20	1.415(3)	1.390	O4-C11-C12	117.8(2)	117.6
N2-C18	1.254(3)	1.269	C16-C11-C12	119.5(2)	119.1
N2-C19	1.468(3)	1.456	O5-C12-C13	125.9(2)	125.8
Compound 2					
O1-C1	1.300(18)	1.302	C7-N1-C8	124.40(15)	124.45
O2-C2	1.367(2)	1.348	O1-C1-C2	120.62(14)	120.55
O3-C9	1.401(2)	1.426	O1-C1-C6	122.79(14)	122.80
N1-C7	1.289(2)	1.279	C2-C1-C6	116.58(14)	116.51
N1-C8	1.457(2)	1.440	O2-C2-C3	119.53(15)	119.55
C1-C2	1.427(2)	1.453	O2-C2-C1	119.07(14)	118.00
C1-C6	1.430(2)	1.417	C3-C2-C1	121.40(15)	121.44
C2-C3	1.368(2)	1.368	C2-C3-C4	121.20(16)	121.23
C3-C4	1.406(3)	1.413	N1- C7-C6	125.14(16)	125.18
C4-C5	1.352(3)	1.340	N1- C8-C9	111.51(15)	111.55
C5-C6	1.422(2)	1.441	O3- C9-C8	108.42(15)	108.44
C6-C7	1.468(3)	1.45	C5- C4-C3	119.56(17)	119.60
C8-C9	1.510(3)	1.50	C4- C5-C6	121.15(17)	121.18

Table 8: Calculated physical parameters of compounds **1** and **2**

Physical properties	**Compound 1**	**Compound 2**
E_{HOMO} (eV)	-5.71	-5.605
E_{LUMO} (eV)	-1.306	-0.952
$\Delta E = E_{HOMO}-E_{LUMO}$ (eV)	4.404	4.653
I.P (eV)	5.71	5.605
E.A (eV)	1.306	0.952
X (eV)	3.508	3.278
η (eV)	2.202	2.326
S (eV^{-1})	0.227	0.215
μ (eV)	-3.508	-3.278
ω (eV^{-1})	-3.508	-3.278
Dipole moment (Debye)	1.68	5.89

Table 9: Antibacterial activity data for compounds **1** and **2**

Pathogen used→ Comp ↓	*S. aureus*	*E. coli*	C-negative *staphylococci*	*K. pneumonia*	*MRSA*
Zone of inhibition in mm (Mean ± standard deviation)					
1	28.52 ± 0.46	16.43 ± 1.03	19.08 ± 1.0	23.85 ± 1.31	14.71 ± 0.54
2	26.72 ± 0.41	19.23 ± 1.05	21.08 ± 1.02	20.75 ± 1.01	16.71 ± 0.34
Cefixime	22.23 ± 0.62	18.04 ± 0.07	15.09 ± 0.82	20.92 ± 1.04	13.4 ± 0.09

Table 10: Antifungal activity data for compounds **1** and **2**

Pathogens used → Comp ↓	*A. niger*	*A. fumigates*	*A. flavus*	*M. species*
Zone of inhibitation in mm (Mean ± standard deviation)				
1	62 ± 1.14	46± 1.18	56± 0.96	76± 1.86
2	69 ± 0.53	38 ± 0.49	61 ± 0.76	65 ± 0.71
Terbinafine	100± 0	100± 0	100± 0	100± 0

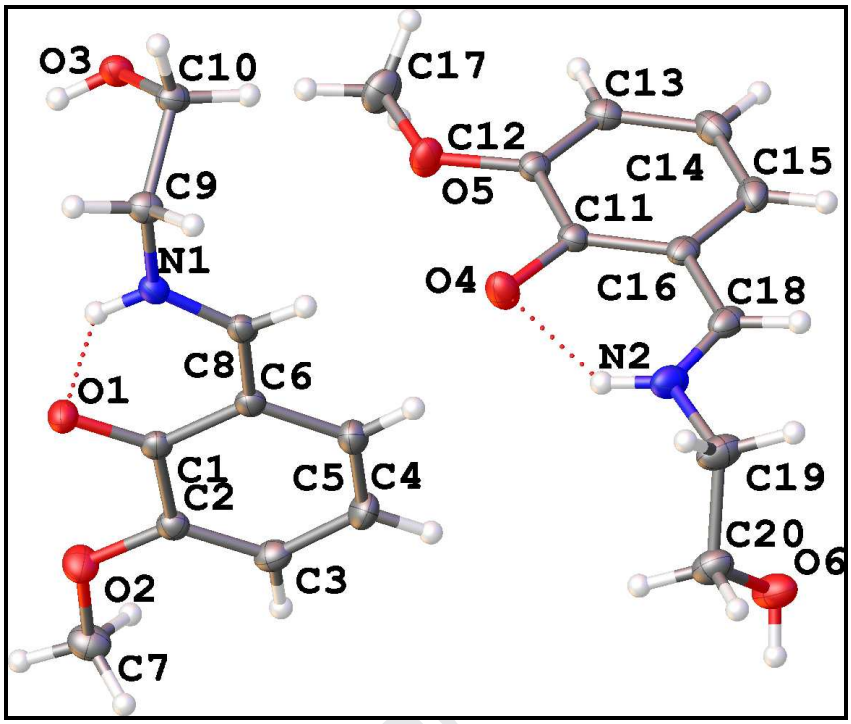

Figure 1: Two independent molecular structures of compound **1** showing atom labeling schemes. The red dotted lines show the N-H…O intermolecular hydrogen bonds which is responsible for Zwitter ion formation in which the H of hydroxyl group is shifted towards N atom

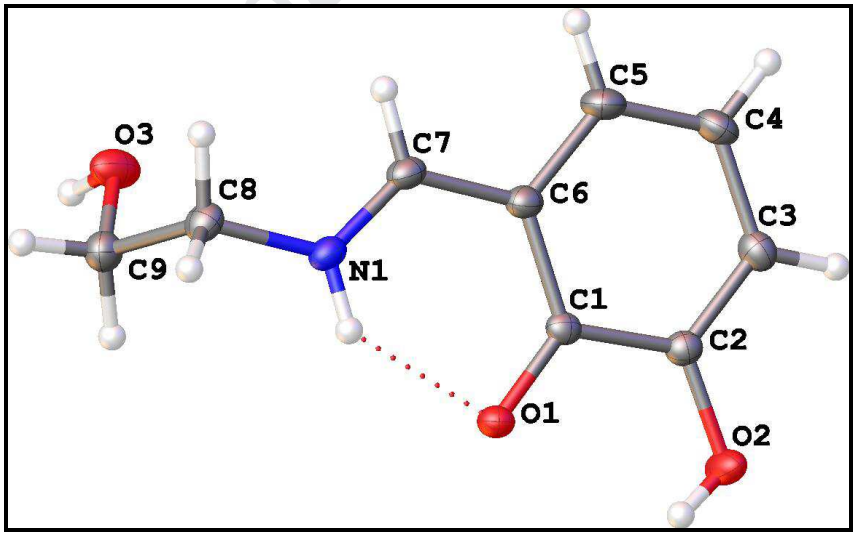

Figure 2: Molecular structures of compound **2** showing atom labeling schemes. The red dotted lines show the N-H…O intermolecular hydrogen bonds which is responsible for Zwitter ion formation in which the H of hydroxyl group is shifted towards N atom

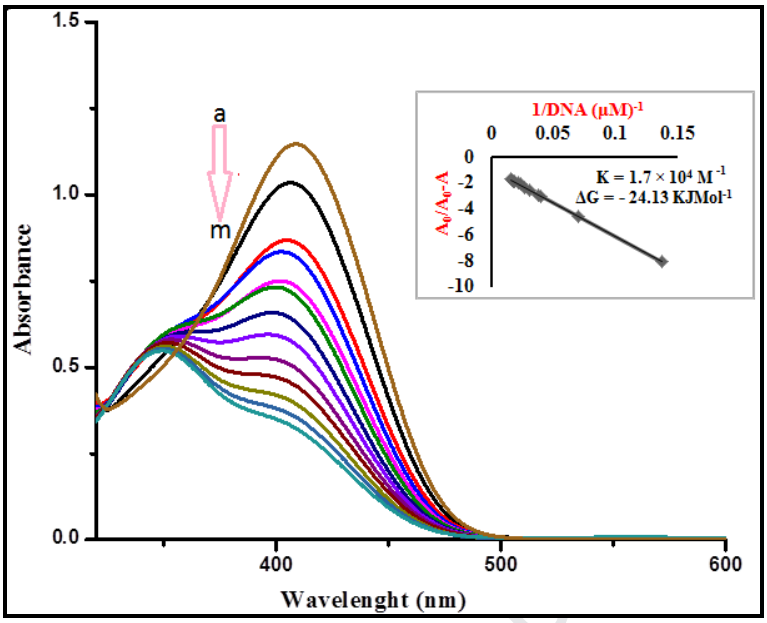

Figure 3: Absorption spectrum of 1mM solution of compound **1** (λ_{max} = 409 nm) in the absence (a) and presence of 8 (b), 16 (c), 24 (d), 32 (e), 40 (f), 48 (g), 56 (h), 64 (i), 72 (j), 80 (k), 88 (l) and 96(m) μM DNA solution. The arrow direction shows the successive increasing conc. of DNA. The inset graph shows binding constant (K) and Gibb's free energy (ΔG).

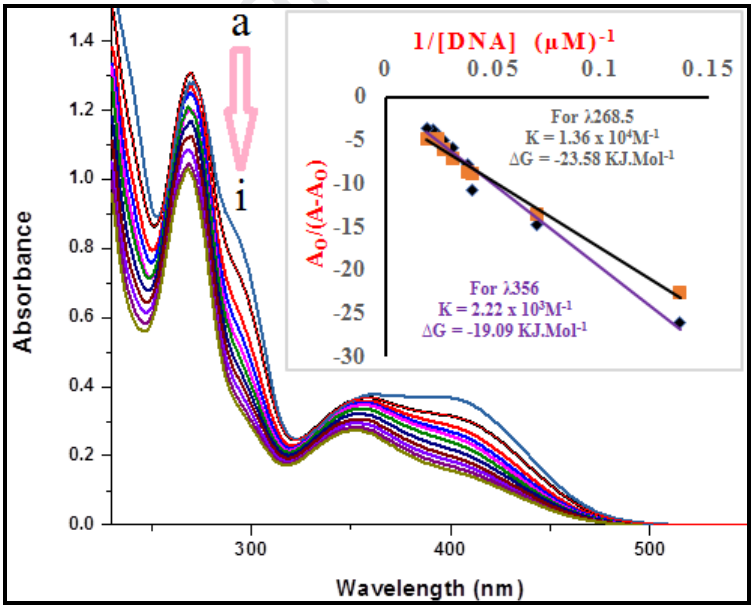

Figure 4: Absorption spectrum of 1mM solution of compound **2** (λ_{max} = 356 nm and 266 nm) in the absence (a) and presence of 8 (b), 16 (c), 24 (d), 32 (e), 40 (f), 48 (g), 56 (h) and 64 (i) μM DNA solution. The arrow direction shows the successive increasing conc. of DNA. The inset graph shows binding constant (K) and Gibb's free energy (ΔG).

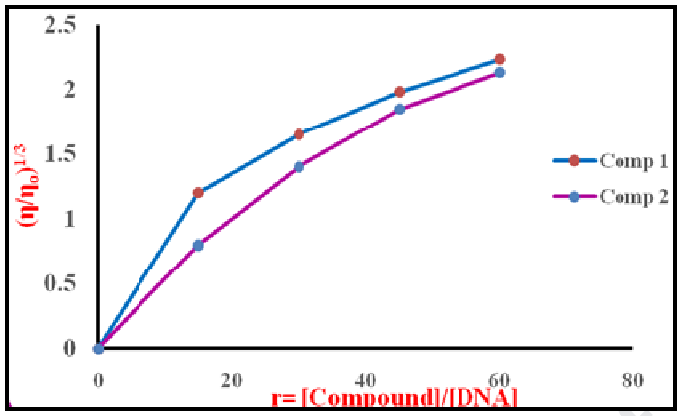

Figure 5: Effect of increasing concentration of compounds **1** and **2** on the relative viscosity of SS-DNA at 25 ± 0.1 °C.

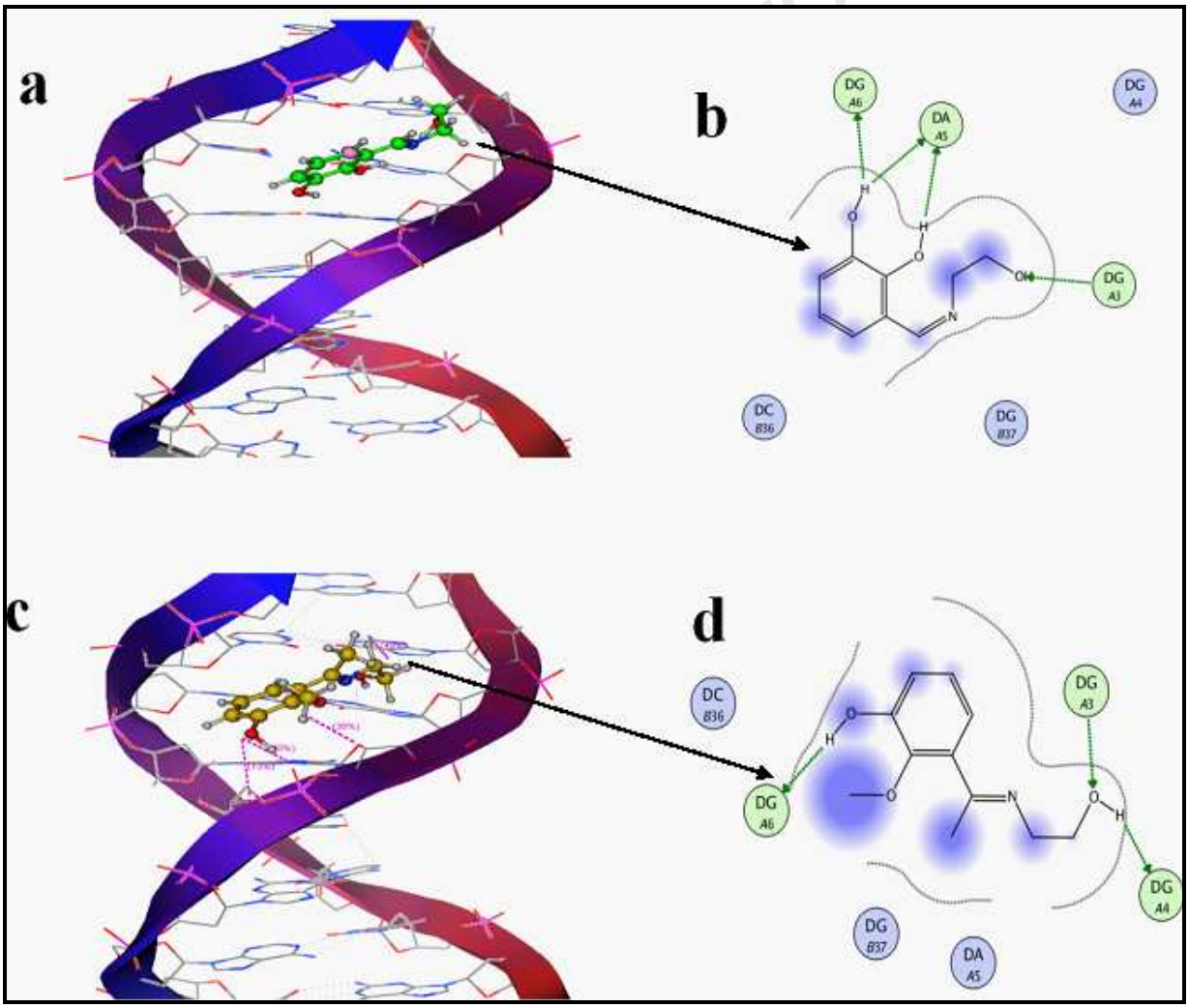

Figure 6: Docked poses of compounds (a) **1** and (b) **2** and 2D molecular interactions of compounds (c) **1** and (b) **2** with nitrogenous bases of DNA.

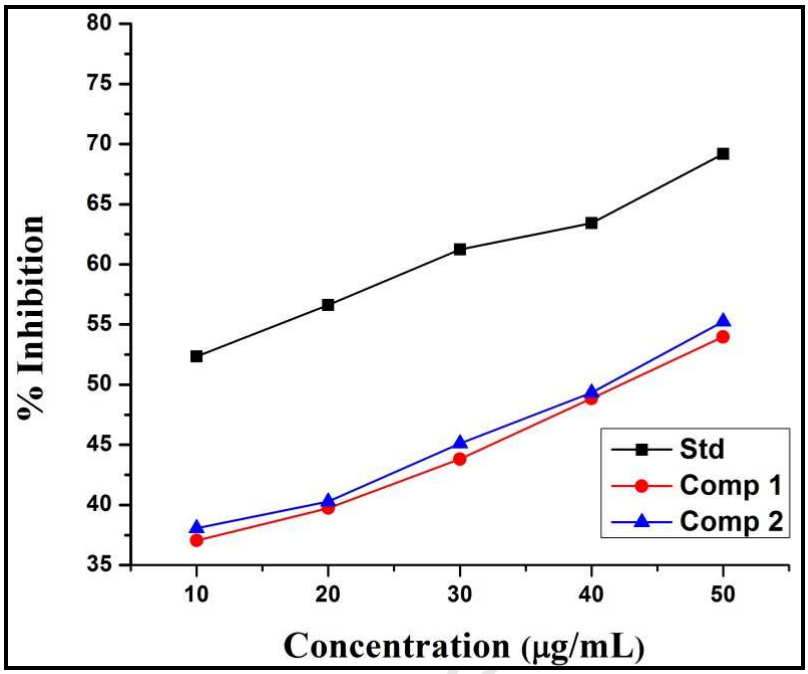

Figure 7: Antioxidant activity of compounds **1** and **2**

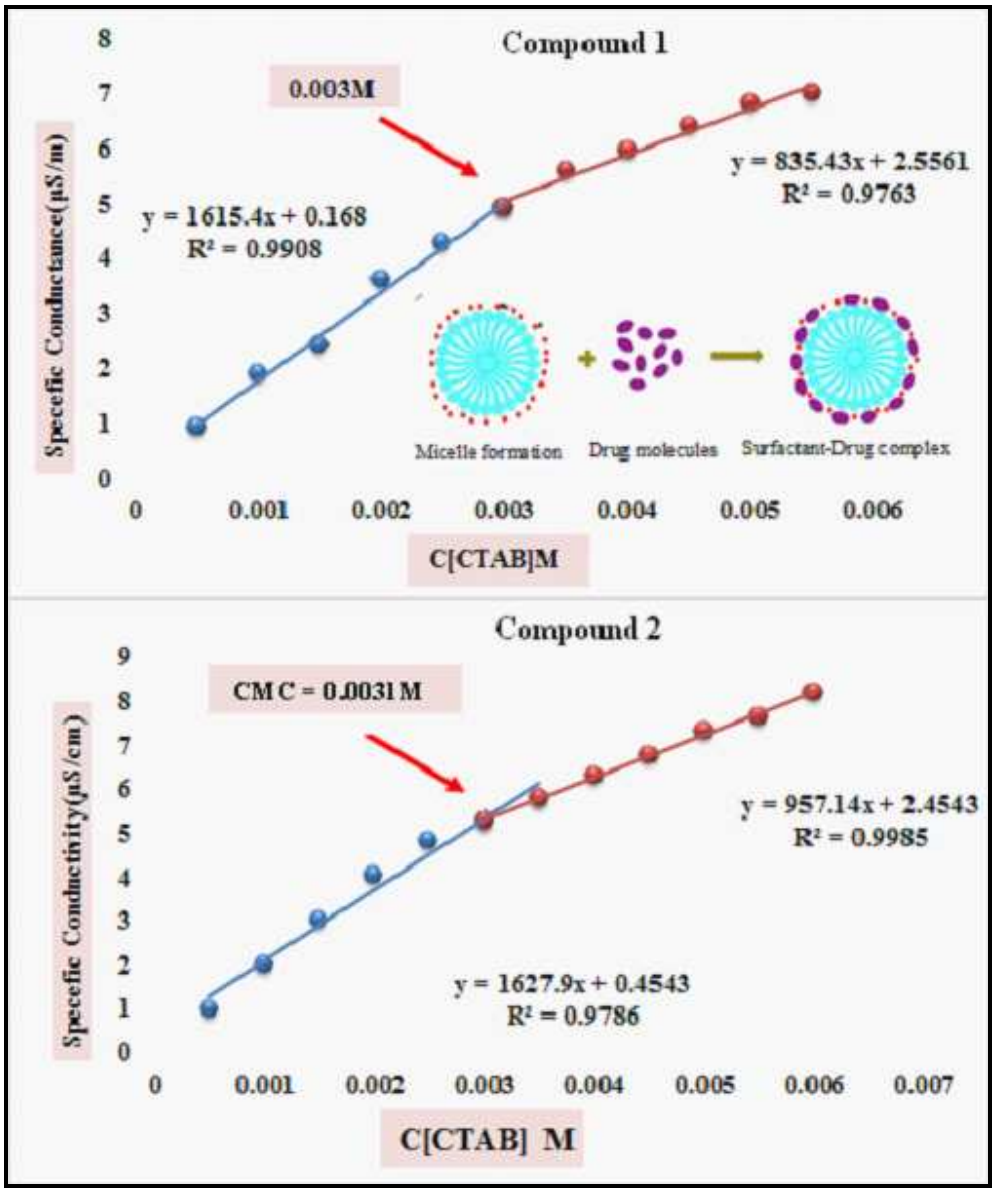

Figure 8: Graph between CTAB-compounds **1** and **2** *vs*. specific conductance

Highlights

- Synthesis of novel azomethines
- Spectroscopic characterizations
- Structural elucidation
- Theoretical study
- Interaction with SS-DNA *via* intercalative mode of interaction
- Antimicrobial and DPPH activities

Author Contribution Statement

Muhammad Zubair: Conceptualization, Methodology, Software, Writing- Original draft preparation

Muhammad Sirajuddin: Data curation, Writing- Reviewing and Editing

Kaleem Ullah: Software

Ali Haider: Editing and checking of data interpretation

Fouzia Perveen: Docking study

Ishtiaq Hussain: Antimicrobial activity

Saqib Ali: Supervision

Muhammad Nawaz Tahir: Crystal analysis

Conflict of interest

There is no conflict of interest